



Effective diffusion barrier layer enables a robust CdSb-based thermoelectric single-leg device



Shanshan Hu¹, Min Liu¹, Long Yang, Zhiwei Chen, Jun Luo , Wen Li ^{*} , Yanzhong Pei ^{**}

Interdisciplinary Materials Research Center, School of Materials Science and Engineering, Tongji University, 4800 Caoan Road, Shanghai, 201804, China

HIGHLIGHTS

- A high-throughput screening strategy identified a barrier layer for CdSb.
- A η_{\max} of 6.5 % for Cd_{0.99}Ag_{0.01}Sb/Ti/Ni single-leg was achieved at $\Delta T \sim 265$ K.
- Cd_{0.99}Ag_{0.01}Sb/Ti/Ni single-leg has excellent thermal stability.

ARTICLE INFO

Keywords:
CdSb
Thermoelectric
Barrier layer
Single-leg device

ABSTRACT

Semiconducting CdSb has been extensively demonstrated to be a highly promising p-type thermoelectric material for low-grade waste heat recovery application. However, achieving chemical stability between this compound and electrodes at elevated temperatures remains a significant challenge, as it is a crucial factor that determines the long-term durability of the generators. The implementation of diffusion barrier layers serves as a viable solution, necessitating that these barriers exhibit exceptional chemical inertness. In this work, the high-throughput screening of twelve metals validates the Ti as a proficient barrier material between the Cd_{0.99}Ag_{0.01}Sb thermoelectric and Ni electrodes, attributed to its low diffusion coefficient and good interfacial contact facilitated by the hot-press sintering. A conversion efficiency of ~6.5 % is achieved for the Cd_{0.99}Ag_{0.01}Sb/Ti/Ni single-leg device at a temperature difference of ~265 K, a value that retains relatively constant during the cyclic measurements with a hot-side temperature of 548 K, which strongly promotes the practical application as a low-cost p-type thermoelectric component in the devices.

1. Introduction

Thermoelectric technique, which facilitates the direct conversion of heat into electricity, has been widely considered as a sustainable solution for addressing energy issues, particularly through the recovery of low-grade waste heat [1–3]. The efficiency of thermoelectric generators is considerably contingent upon the thermoelectric performance of the constituent materials, as well as the quality of the interfacial contact between the materials and the electrodes [4,5]. In recent decades, significant breakthroughs with zT exceeding 2.0 have been frequently realized in a variety of thermoelectric materials, including PbTe [6], GeTe [7], SnSe [8], AgSbTe₂ [9] and Cu₂Se [10]. Such advancements can be achieved by the band [11–13] and defect [14–16] engineering.

These findings stimulate significant endeavors towards the development of highly efficient thermoelectric devices.

Besides the exceptional thermoelectric performance, the interfacial interaction between thermoelectric materials and electrodes assumes a pivotal role in the realization of high-performance devices [17]. It is imperative that these interfaces exhibit thermal stability, robust bonding strength, and minimal electrical and thermal resistivity [18]. Given the relatively elevated temperatures experienced by the hot side of the device, ensuring chemical stability becomes a primary concern. Poor stability can lead to an undesirable increase in specific contact resistivity and possibly compromise the integrity of the interfacial bonding [19].

Note that typical weldable electrode materials, such as Cu [20,21],

* Corresponding author.

** Corresponding author.

E-mail addresses: liwen@tongji.edu.cn (W. Li), yanzhong@tongji.edu.cn (Y. Pei).

¹ These authors contributed equally.

Ag [22] and Ni [23,24], have been shown to serve as effective dopants in most thermoelectric materials. The direction contacts between these electrodes and thermoelectric materials often result in significant degradation of device efficiency due to their reactivity [19]. Therefore, the introduction of a barrier layer, which exhibits inertness to both thermoelectric materials and electrodes, has been proposed and proven to be an available pathway for mitigating the degradation of the devices [25,26]. In further detail, the Cr [27], Co²⁸, Ti [28], NiGe [29] and MgCuSb [30] are identified as suitable barrier materials for half-Heusler, PbTe, Bi₂Te₃, GeTe and MgAgSb, respectively, in order to impede diffusion and reactions.

Due to its intrinsically low lattice thermal conductivity, semiconducting CdSb has emerged as a promising p-type thermoelectric material, demonstrating impressive zT of ~0.4 and ~1.2 at 300 K and 550 K, respectively [31]. These elucidate its significant potential for the utilization of low-grade waste heat recovery applications. An efficiency exceeding 8 % has been achieved in the CdSb/Mg₃SbBi modules at a temperature difference of 270 K [32]. Antimony (Sb) is employed as the barrier layer, however, thermal cycling measurements reveal a noticeable increase in the interfacial contact resistivity. Therefore, it is essential to explore alternative barrier materials that exhibit inertness toward the CdSb thermoelectric material.

In this work, a high-throughput screening strategy is applied to identify an optimal barrier material from a selection of twelve metals. Titanium (Ti) emerges as a highly effective barrier material between CdSb thermoelectric material and Ni electrode due to its low diffusion coefficient and excellent interfacial contact properties. The interfacial contact resistivity is measured to be as low as ~55 $\mu\Omega$ cm². Consequently, the CdSb/Ti/Ni single-leg device achieves a conversion efficiency of ~6.5 % at a temperature difference of ~265 K. This efficiency remains stable even after thermal cycling tests at a hot-end temperature of 548 K.

2. Materials and methods

Polycrystalline Cd_{0.99}Ag_{0.01}Sb samples were synthesized by melting stoichiometric high-purity (>99.99 %) elements Cd, Ag and Sb in a vacuum-protected quartz tube at 873 K for 5 h with a heating rate of 150 °C/min, followed by quenching in cold water and annealing at 673 K for two days, after which the samples were again quenched in cold water. The resulting ingots were manually ground into fine powders for phase composition analysis using X-ray diffraction (XRD) and for pellet preparation through hot-pressing. The Cd_{0.99}Ag_{0.01}Sb powders, both with and without a mixture of twelve candidate barrier metals (Fe, Co, Ni, Ag, Ti, V, Cr, Zr, Nb, Mo, Ta, W) (>99.9 %), were then sintered into dense pellets (>98.5 % theoretical density) via hot pressing at 658 K for 90 min under a uniaxial pressure of ~65 MPa. The obtained pellets were ~12 mm in diameter and ~1.5 mm in thickness.

The mixed pellets underwent additional aging at 573 K for 36, 324 and 400 h under vacuum to examine the interfacial microstructures and determine the diffusion coefficients for various metals. The microstructures and compositions were analyzed using a scanning electron microscope (SEM) equipped with an energy dispersive spectrometer (EDS). The diffusion coefficient for the metals were calculated based on the concentration distribution of metals versus diffusion distance at different aging times, following the Fick's second law [33]. Details on estimating the diffusion coefficient of the metals and measuring transport properties such as Hall coefficient (R_H), resistivity (ρ), Seebeck coefficient (S) and thermal diffusivity (D) for Cd_{0.99}Ag_{0.01}Sb pellets can be found in our previous work [31,32]. Thermal conductivity (κ) was determined via $\kappa = dC_p D$, where d and C_p represent density estimated by mass/volume and specific heat determined by the Dulong-Petit limit, assuming temperature independence. The thermal diffusivity was tested by the Flash Method in accordance with ASTM 1461.

Ni/Ti/Cd_{0.99}Ag_{0.01}Sb/Ti/Ni cylinders with a dimension of ~12 mm in diameter and ~5.5 mm in thickness were fabricated by a one-step hot

pressing using powders of Cd_{0.99}Ag_{0.01}Sb, Ti and Ni (Ti layer: ~0.1 mm, Ni layer: ~0.65 mm, with a particle size of 300 mesh). The fabrication was conducted at a temperature of 658 K, under a pressure of ~65 MPa for 90 min (schematically shown in Fig. S1a). The resulting bulks were then cut into thermoelectric legs with sizes of 1.7 mm × 1.7 mm × 5.5 mm for the measurement of interfacial contact resistance (R_c) and efficiency (η). Moreover, the legs were annealed at 573 K for 72, 168 and 216 h under vacuum to examine the chemical diffusion/reaction and the interfacial bonding. The R_c was measured using a four-probe technique. The η of the single-leg devices was measured by a home-made efficiency system (schematically shown in Fig. S1b), where the legs were loaded between the heater and the heat-flow meter using liquid metals. Two K-type thermocouples, labeled as T_1 and T_2 , were embedded at two sides of the leg to measure both the temperature difference and output voltage. The copper bar (cross-sectional area of 3 × 3 mm²) was used as a heat-flow meter and two K-type thermocouples (T_3 and T_4) with a small diameter of 0.06 mm were embedded to determine the temperature difference. The copper heater and copper bar functioned as the electrodes to measure the current.

3. Results and discussions

Room temperature powder XRD result for Cd_{0.99}Ag_{0.01}Sb, shown in Fig. S2a, signifies the formation of a single phase, which is further identified by the SEM image showing no additional precipitates and the EDS mapping demonstrating a uniform elemental distribution (Fig. S2b). The transport properties of Cd_{0.99}Ag_{0.01}Sb are illustrated in Fig. S3 and Fig. 1a–b. The obtained samples exhibit a Hall carrier concentration of 9.5×10^{18} cm⁻³ (Fig. S3a), which is consistent with the literature [31]. The reductions in resistivity and Seebeck coefficient above 450 K are attributed to the bipolar effect (Figs. S3b–c). A power factor exceeding 13 $\mu\text{W}/\text{cm}\cdot\text{K}^2$ is attained at 300 K, which increases to ~18 $\mu\text{W}/\text{cm}\cdot\text{K}^2$ with increasing temperature (Fig. S3d).

The determination of κ_L involves subtracting the electronic contribution (κ_E), as dictated by the Wiedemann-Franz law ($\kappa_E = LT/\rho$), from the overall thermal conductivity (κ). Here, the Lorentz factor (L) is determined using the single parabolic band (SPB) model, taking into account acoustic phonon scattering. With the κ_L consistently below 1.0 across the entire temperature range (Fig. S3e), a peak zT as high as 1.2 and an average zT_{ave} of ~0.93 within 300~600 K are realized for Cd_{0.99}Ag_{0.01}Sb, as shown in Fig. 1a–b and Fig. S3f. Although such a thermoelectric performance is still significantly lower than that of GeTe-based and AgSbTe₂-based thermoelectric materials, it is comparable to that of Bi₂Te₃-based thermoelectric materials, indicating that this compound holds great promise as a viable candidate for the application of low-grade waste heat recovery.

It is known that establishing a dependable interfacial connection between the thermoelectric material and the electrode is crucial for ensuring the longevity of the devices. Twelve metal powders (Fe, Co, Ni, Cu, Ti, V, Cr, Zr, Ni, Mo, Ta, and W) are sintered into a Cd_{0.99}Ag_{0.01}Sb matrix to identify thermally stable barrier materials. The interfaces of these materials are characterized and illustrated in Fig. 2, as well as in Figs. S4 and S5. The diffusions of Fe, Co, Ni and Cu in the matrix are notably observed in Fig. S4, which enable the formation of interphases as FeSb₂ [41], CoSb₃ [42], NiSb [43] and Ag₅Cd₈ [44], respectively. The interphases that are formed could potentially cause expansion or shrinkage of the volume, ultimately resulting in cracking of the legs [24]. This suggests that the aforementioned four metals are not advisable as barrier materials for Cd_{0.99}Ag_{0.01}Sb, as the interfaces may deteriorate or even fail under extended periods of high-temperature operation and thermal cycling.

Cd_{0.99}Ag_{0.01}Sb is suitable for being designed to operate within the temperature range of 300–550 K for power generation [32]. The remaining metals are further aged at 573 K for 36, 324 and 400 h under vacuum to elucidate the thermal stability. The stability is qualitatively analyzed through SEM observations and quantitatively assessed based

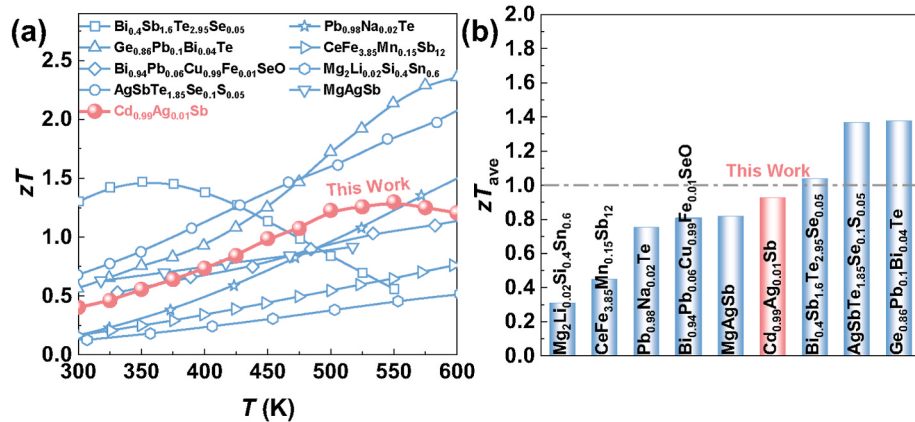


Fig. 1. Figure of merit (zT) versus temperature (a) & average zT_{ave} (b) [7,34–40] for $\text{Cd}_{0.99}\text{Ag}_{0.01}\text{Sb}$, with a comparison to the typical high-performance p-type thermoelectric materials.

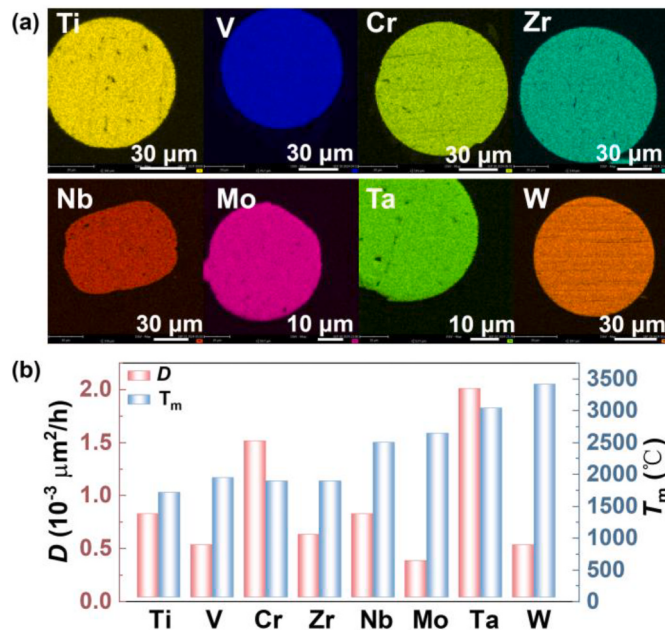


Fig. 2. EDS mapping images showing the interfaces between eight barrier candidates and matrix after hot pressing and aging at 573 K for up to 400 h (Ti, V, Cr, Zr, Nb, Mo, Ta, W) (a) and their diffusion coefficient in $\text{Cd}_{0.99}\text{Ag}_{0.01}\text{Sb}$ and melting point [45] (b).

on the diffusion coefficient (D). The SEM images and corresponding EDS analyses for the interfaces between the barrier candidates and the matrix are presented in Fig. 2a and Figs. S5–S6. The distinct interfaces between the metals and the thermoelectric material indicate their chemical inertness.

As shown in Fig. S7, the ratio of diffusion distance (x) to the square root of aging time t (x/\sqrt{t} with a unit of $\mu\text{m}/\text{h}^{1/2}$), as determined by the EDS compositional line scans, effectively characterizes the spatial concentration distribution of the diffusers across significantly varied aging times. The D of various metals in $\text{Cd}_{0.99}\text{Ag}_{0.01}\text{Sb}$ are quantitatively estimated using Fick's second law [33] from diffusion curves after aging, as shown in Fig. 2b. The D of the metals are estimated to be smaller than $2.0 \times 10^{-3} \mu\text{m}^2/\text{h}$, whereas Ta and Cr exhibit significantly higher values compared to Ti, Nb, Zr, V, W, Mo. The low diffusion coefficient between these metals and $\text{Cd}_{0.99}\text{Ag}_{0.01}\text{Sb}$ suggest a long-term thermal stability for CdSb-based devices.

Considering the sinterability for both thermoelectric material and electrode, the Ti, which shows the lowest melting point among them

(Fig. 2b), is selected as the barrier material for assembling $\text{Cd}_{0.99}\text{Ag}_{0.01}\text{Sb}$ single-leg devices. In addition to their chemical inertness, the establishment of strong bonds that facilitate excellent electrical and thermal conductivity is imperative for an optimal electrode material, which promotes the Ti, showing the lowest melting point among the materials (Fig. 2b), as the barrier material in CdSb. Consequently, the $\text{Cd}_{0.99}\text{Ag}_{0.01}\text{Sb}/\text{Ti}/\text{Ni}$ joint is fabricated by a one-step hot pressing process, and the specific interfaces of Ni/Ti and $\text{Cd}_{0.99}\text{Ag}_{0.01}\text{Sb}/\text{Ti}$ are characterized by the SEM observation, as shown in Fig. 3. The SEM image and EDS mapping reliably demonstrate well-established bonding at both interfaces, with negligible diffusion or reaction (Fig. 3a), this finding is further substantiated by the EDS line scanning (Fig. 3b), which reveals distinct boundaries. The further aging at 573 K for 72, 168 and 216 h suggests the thermal stability of the interfaces (Fig. S8). The electrical contact resistance (R_c) for the $\text{Cd}_{0.99}\text{Ag}_{0.01}\text{Sb}/\text{Ti}/\text{Ni}$ joint with a size of $1.7 \text{ mm} \times 1.7 \text{ mm} \times 5.5 \text{ mm}$ is measured by a four-probe technique (as schematically shown in the inset of Fig. 3c). The R_c is measured to be $1.83 \text{ m}\Omega$ and $1.98 \text{ m}\Omega$ at both ends of the leg, which correspond to the electrical contact resistivity (ρ_c) of $52.9 \text{ }\Omega \text{ cm}^2$ and

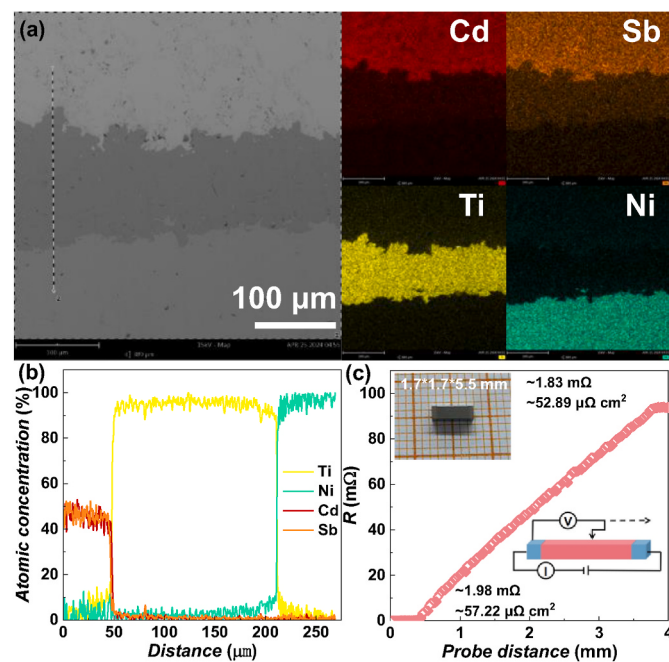


Fig. 3. SEM image with corresponding EDS mapping (a) and line scan (b) and line scan resistance across the joint (c) of Ni/Ti/ $\text{Cd}_{0.99}\text{Ag}_{0.01}\text{Sb}$.

57.2 $\Omega \text{ cm}^2$, respectively, as shown in Fig. 3c.

The single-leg devices with a size of 1.7 mm \times 1.7 mm \times 5.5 mm are cut for measuring the power output (P) and efficiency (η), as shown in Fig. 4. Based on the resistivity of the thermoelectric material and the interfacial contact resistivity, the predicted total contact resistance at both sides is approximately 10 % of the internal resistance (R_{in}) of the device. This suggests a favorable P and η under applied temperature gradients (ΔT). For the efficiency measurement, the cold side temperature is maintained at 300 K. Fig. 4a shows the output voltage (V) versus current (I) for Cd_{0.99}Ag_{0.01}Sb single-leg devices with barrier layers under varying ΔT . The linear nature of the V - I curves allows for the determination of the open circuit voltage (V_{oc}) and the R_{in} through linear fitting, with the intercept and slope corresponding to these parameters, respectively. The increase in V_{oc} with rising ΔT is attributed to the enhanced Seebeck coefficient at elevated temperatures.

The P and η under different temperature gradients (ΔT) for Cd_{0.99}Ag_{0.01}Sb single-leg devices with barrier layers and electrodes are shown in Fig. 4b and c, respectively. The measurement schematic is illustrated in the inset of Fig. 4c. A maximum P_{max} of \sim 20 mW is obtained at a ΔT of \sim 265 K (Fig. 4b). As a result, a maximum efficiency η_{max} of \sim 6.5 % is realized at $\Delta T = 265$ K. The stability of the performance is further validated through the consistent performance of another single-leg device (Figs. S9a–S9c). To illustrate the potential of the Cd_{0.99}Ag_{0.01}Sb device, the legs devoid of barrier layers and electrodes is loaded between the heater and the heat-flow meter using liquid alloy as the conductive paste, where the metal heater block and the Cu heat-flow meter serve as the electrodes for measuring the output current. This approach effectively mitigates the impact of interfacial resistance on both P and η . The corresponding results are shown in Fig. 4d–f and Figs. S9d–f. The maximum P_{max} and η_{max} of \sim 22.5 mW

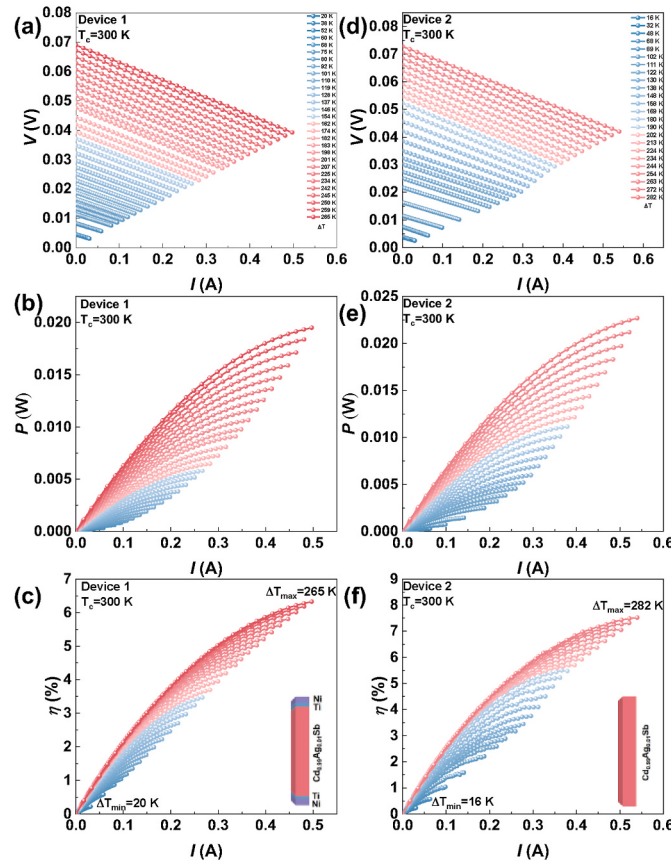


Fig. 4. Output voltage (a, d), output power (b, e) and efficiency (c, f) versus current for Cd_{0.99}Ag_{0.01}Sb devices with (a, b, c) and without (d, e, f) barrier layers and electrodes.

(Fig. 4e) and \sim 7.5 % (Fig. 4f) are achieved at a ΔT of \sim 282 K, respectively, enabling \sim 10 % enhancements in the overall power output and efficiency due to the exclusion of interfacial contact.

The long-term measurements, illustrated in Fig. 5a, reveal no observable degradations in η_{max} , P_{max} , V_{oc} and R_{in} for Ni/Ti/Cd_{0.99}Ag_{0.01}Sb/Ti/Ni single-leg device, while the R_{in} of the Ni/Cd_{0.99}Ag_{0.01}Sb/Ni single-leg device without Ti barrier layer increased significantly (Fig. S10). Moreover, the V_{oc} for the device without Ti barrier layer is found to be nearly constant, which implies the thermal stability of the thermoelectric material at 548 K. Therefore, the increase in its R_{in} can be reasonably attributed to the increase in the interfacial contact resistance (R_c). These results provide further evidence of the thermal stability of the Cd_{0.99}Ag_{0.01}Sb/Ti joint and the thermoelectric material. Additionally, the obtained maximum η_{max} for the Cd_{0.99}Ag_{0.01}Sb device in this work ranks among the highest reported p-type thermoelectric single-leg devices at temperature below 550 K^[39,40,46,47,48,49,50]. This observation underscores the potential of this material as a promising p-type component for the thermoelectric generators aimed at harnessing low-grade heat.

4. Summary

In summary, a high-throughput way is employed to reveal the diffusion behavior at the interfaces between Cd_{0.99}Ag_{0.01}Sb and twelve metals considered as barrier materials. The low diffusion coefficients unveil the chemical inertness of Ti, V, Cr, Zr, Ni, Mo, Ta, and W toward Cd_{0.99}Ag_{0.01}Sb, thereby identifying them as potential barrier materials. Considering the sinterability in relation to the melting point, Ti is chosen to fabricate Cd_{0.99}Ag_{0.01}Sb single-leg devices for evaluating the efficiency and its thermal stability. A maximal efficiency of 6.5 % is achieved in Ni/Ti/Cd_{0.99}Ag_{0.01}Sb/Ti/Ni single-leg devices at a temperature difference of \sim 265 K, and its thermal stability is validated by the absence of performance degradation during long-term measurements. These results firmly demonstrate Ni/Ti/Cd_{0.99}Ag_{0.01}Sb/Ti/Ni single-leg as a promising and cost-effective p-type component in thermoelectric generators for recovering low-grade heat.

CRediT authorship contribution statement

Shanshan Hu: Writing – original draft, Investigation. **Min Liu:** Resources, Methodology. **Long Yang:** Formal analysis. **Zhiwei Chen:** Formal analysis. **Jun Luo:** Methodology, Formal analysis. **Wen Li:** Writing – review & editing, Supervision. **Yanzhong Pei:** Supervision, Project administration, Conceptualization.

Declaration of competing interest

The authors declare that they have no known competing financial

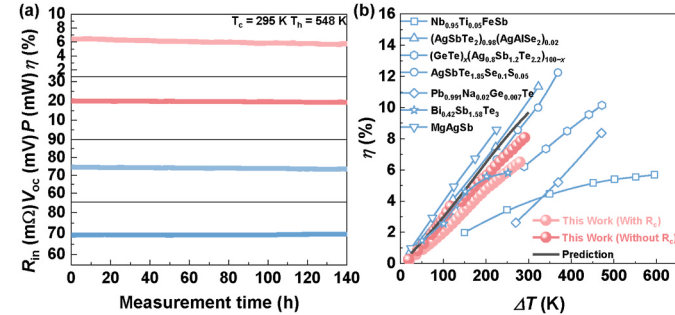


Fig. 5. Maximum efficiency (η_{max}), maximum output power (P_{max}), open circuit voltage (V_{oc}) and internal resistance (R_{in}) for Ni/Ti/Cd_{0.99}Ag_{0.01}Sb/Ti/Ni device during the long-term measurements (a), and temperature-difference dependent maximum efficiency for the devices, with a comparison to the prediction and the literature results [39,40,46–50] (b).

interests or personal relationships that could have appeared to influence the work reported in this paper.

Acknowledgments

This work was supported by the National Key Research and Development Program of China (2023YFB3809400), the National Natural Science Foundation of China (Grant Nos. T2125008, 92163203 and 52371234), the Innovation Program of Shanghai Municipal Education Commission (202101-07-00-07-E00096), the Hong Kong, Macao and Taiwan Science and Technology Cooperation Project for Science and Technology Innovation Plan of Shanghai (23520760600) and the Fundamental Research Funds for the Central Universities.

Appendix A. Supplementary data

Supplementary data to this article can be found online at <https://doi.org/10.1016/j.jpowsour.2024.236102>.

Data availability

Data will be made available on request.

References

- [1] F.J. DiSalvo, Thermoelectric cooling and power generation, *Science* 285 (5428) (1999) 703–706.
- [2] L.E. Bell, Cooling, heating, generating power, and recovering waste heat with thermoelectric systems, *Science* 321 (5895) (2008) 1457–1461.
- [3] A. El-Khouly, A. Novitskii, I. Serhiienko, A. Kalugina, A. Sedegov, D. Karpenkov, A. Voronin, V. Khovaly, A.M. Adam, Optimizing the thermoelectric performance of FeVSb half-Heusler compound via Hf-Ti double doping, *J. Power Sources* 477 (2020) 228768.
- [4] Q. Zhu, S. Song, H. Zhu, Z. Ren, Realizing high conversion efficiency of Mg₃Sb₂-based thermoelectric materials, *J. Power Sources* 414 (2019) 393–400.
- [5] A. Nozariasbmarz, U. Saparamadu, W. Li, H.B. Kang, C. Dettor, H. Zhu, B. Poudel, S. Priya, High-performance half-Heusler thermoelectric devices through direct bonding technique, *J. Power Sources* 493 (2021) 229695.
- [6] Z. Chen, Z. Jian, W. Li, Y. Chang, B. Ge, R. Hanus, J. Yang, Y. Chen, M. Huang, G. J. Snyder, Y. Pei, Lattice dislocations enhancing thermoelectric PbTe in addition to band convergence, *Adv. Mater.* 29 (23) (2017) 1606768.
- [7] J. Li, X. Zhang, Z. Chen, S. Lin, W. Li, J. Shen, I.T. Witting, A. Faghaninia, Y. Chen, A. Jain, L. Chen, G.J. Snyder, Y. Pei, Low-symmetry rhombohedral GeTe thermoelectrics, *Joule* 2 (5) (2018) 976–987.
- [8] D. Liu, D. Wang, T. Hong, Z. Wang, Y. Wang, Y. Qin, L. Su, T. Yang, X. Gao, Z. Ge, B. Qin, L.-D. Zhao, Lattice plainification advances highly effective SnSe crystalline thermoelectrics, *Science* 380 (6647) (2023) 841–846.
- [9] S. Roychowdhury, T. Ghosh, R. Arora, M. Samanta, L. Xie, N.K. Singh, A. Soni, J. He, U.V. Waghmare, K. Biswas, Enhanced atomic ordering leads to high thermoelectric performance in Ag₃SbTe₂, *Science* 371 (6530) (2021) 722–727.
- [10] W.-D. Liu, L. Yang, Z.-G. Chen, Cu₂Se thermoelectrics: property, methodology, and device, *Nano Today* 35 (2020) 100938.
- [11] H.-X. Liu, X.-Y. Zhang, Z.-L. Bu, W. Li, Y.-Z. Pei, Thermoelectric properties of (GeTe)_{1-x}(Ag₂Te)_{0.4}(Sb₂Te₃)_{0.6}_x alloys, *Rare Met.* 41 (3) (2022) 921–930.
- [12] Y.-J. Fan, K.-L. Peng, Y.-L. Huang, H.-J. Liao, Z.-Y. Huang, J. Li, Y.-C. Yan, H.-S. Gu, B. Zhang, Y.-M. Hu, X. Lu, X.-Y. Zhou, Enhanced thermoelectric performance of Cu₂SnSe₃ via synergistic effects of Cd-doping and CuGaTe₂ alloying, *Rare Met.* 41 (10) (2022) 3466–3474.
- [13] Y. Pei, X. Shi, A. LaLonde, H. Wang, L. Chen, G.J. Snyder, Convergence of electronic bands for high performance bulk thermoelectrics, *Nature* 473 (7345) (2011) 66–69.
- [14] K.-J. Liu, Z.-W. Zhang, C. Chen, L.-H. Wei, H.-L. He, J. Mao, Q. Zhang, Entropy engineering in CaZn₂Sb₂-YbMg₂Sb₂ Zintl alloys for enhanced thermoelectric performance, *Rare Met.* 41 (9) (2022) 2998–3004.
- [15] M.-F. Wang, H.-J. Lai, J.-S. Liang, J.-L. Chen, W.-Y. Ding, Q. Zhou, Y. Peng, C.-Y. Liu, L. Miao, Enhanced thermoelectric performance enabled by compositing ZrO₂ in n-type SiGe alloy with low thermal conductivity, *Rare Met.* 43 (3) (2024) 1167–1176.
- [16] R.-S. Zhai, T.-J. Zhu, Improved thermoelectric properties of zone-melted p-type bismuth-telluride-based alloys for power generation, *Rare Met.* 41 (5) (2022) 1490–1495.
- [17] W. Liu, S. Bai, Thermoelectric interface materials: a perspective to the challenge of thermoelectric power generation module, *J. Mater.* 5 (3) (2019) 321–336.
- [18] W. Wu, G.-K. Ren, X. Chen, Y. Liu, Z. Zhou, J. Song, Y. Shi, J.-M. Jiang, Y.-H. Lin, Interfacial advances yielding high efficiencies for thermoelectric devices, *J. Mater. Chem. A* 9 (6) (2021) 3209–3230.
- [19] R. He, G. Schiering, K. Nielsch, Thermoelectric Devices: a review of devices, architectures, and contact optimization, *Adv. Mater. Technol.* 3 (4) (2018) 1700256.
- [20] L.-C. Yin, W.-D. Liu, M. Li, D.-Z. Wang, H. Wu, Y. Wang, L. Zhang, X.-L. Shi, Q. Liu, Z.-G. Chen, Interstitial Cu: an effective strategy for high carrier mobility and high thermoelectric performance in GeTe, *Adv. Funct. Mater.* 33 (25) (2023) 2301750.
- [21] Y. Xiao, H. Wu, W. Li, M. Yin, Y. Pei, Y. Zhang, L. Fu, Y. Chen, S.J. Pennycook, L. Huang, J. He, L.-D. Zhao, Remarkable roles of Cu to synergistically optimize phonon and carrier transport in n-type PbTe-Cu₂Te, *J. Am. Chem. Soc.* 139 (51) (2017) 18732–18738.
- [22] C.-L. Chen, H. Wang, Y.-Y. Chen, T. Day, G.J. Snyder, Thermoelectric properties of p-type polycrystalline SnSe doped with Ag, *J. Mater. Chem. A* 2 (29) (2014) 11171–11176.
- [23] P.F. Qiu, R.H. Liu, J. Yang, X. Shi, X.Y. Huang, W. Zhang, L.D. Chen, J. Yang, D. J. Singh, Thermoelectric properties of Ni-doped CeFe₄Sb₁₂ skutterudites, *J. Appl. Phys.* 111 (2) (2012) 023705.
- [24] X. Lu, D.T. Morelli, Y. Xia, V. Ozolins, Increasing the thermoelectric figure of merit of tetrahedrites by Co-doping with nickel and zinc, *Chem. Mater.* 27 (2) (2015) 408–413.
- [25] J. Chu, J. Huang, R. Liu, J. Liao, X. Xia, Q. Zhang, C. Wang, M. Gu, S. Bai, X. Shi, L. Chen, Electrode interface optimization advances conversion efficiency and stability of thermoelectric devices, *Nat. Commun.* 11 (1) (2020) 2723.
- [26] W. Zhu, P. Wei, J. Zhang, L. Li, W. Zhu, X. Nie, X. Sang, Q. Zhang, W. Zhao, Fabrication and excellent performances of bismuth telluride-based thermoelectric devices, *Acs Appl. Mater. Interfac.* 14 (10) (2022) 12276–12283.
- [27] R. Liu, Y. Xing, J. Liao, X. Xia, C. Wang, C. Zhu, F. Xu, Z.-G. Chen, L. Chen, J. Huang, S. Bai, Thermal-inert and ohmic-contact interface for high performance half-Heusler based thermoelectric generator, *Nat. Commun.* 13 (1) (2022) 7738.
- [28] M. Liu, W. Li, Y. Pei, Screening metal diffusion barriers for thermoelectric Bi_{0.5}Sb_{1.5}Te₃, *Sci. China Mater.* 67 (1) (2024) 289–294.
- [29] L. Xie, C. Ming, Q. Song, C. Wang, J. Liao, L. Wang, C. Zhu, F. Xu, Y.-Y. Sun, S. Bai, L. Chen, Lead-free and scalable GeTe-based thermoelectric module with an efficiency of 12, *Sci. Adv.* 9 (27) (2023) 7919.
- [30] L. Xie, L. Yin, Y. Yu, G. Peng, S. Song, P. Ying, S. Cai, Y. Sun, W. Shi, H. Wu, N. Qu, F. Guo, W. Cai, H. Wu, Q. Zhang, K. Nielsch, Z. Ren, Z. Liu, J. Sui, Screening strategy for developing thermoelectric interface materials, *Science* 382 (6673) (2023) 921–928.
- [31] B. Zhou, C. Sun, X. Wang, Z. Bu, W. Li, R. Ang, Y. Pei, Transport properties of CdSb alloys with a promising thermoelectric performance, *Acs Appl. Mater. Interfac.* 11 (30) (2019) 27098–27103.
- [32] Z. Bu, X. Zhang, Y. Hu, Z. Chen, S. Lin, W. Li, C. Xiao, Y. Pei, A record thermoelectric efficiency in tellurium-free modules for low-grade waste heat recovery, *Nat. Commun.* 13 (1) (2022) 921–928.
- [33] M. Liu, X. Zhang, Y. Wu, Z. Bu, Z. Chen, W. Li, Y. Pei, Screening metal electrodes for thermoelectric PbTe, *Acs Appl. Mater. Interfac.* 15 (4) (2023) 6169–6176.
- [34] Q. Zhang, M. Yuan, K. Pang, Y. Zhang, R. Wang, X. Tan, G. Wu, H. Hu, J. Wu, P. Sun, G.-Q. Liu, J. Jiang, High-performance industrial-grade p-type (Bi,Sb)₂Te₃ thermoelectric enabled by a stepwise optimization strategy, *Adv. Mater.* 35 (21) (2023) 2300338.
- [35] G. Tan, F. Shi, S. Hao, L.-D. Zhao, H. Chi, X. Zhang, C. Uher, C. Wolverton, V. P. Dravid, M.G. Kanatzidis, Non-equilibrium processing leads to record high thermoelectric figure of merit in PbTe-SrTe, *Nat. Commun.* 7 (2016) 12167.
- [36] P. Qiu, X. Shi, R. Liu, Y. Qiu, S. Wan, L. Chen, Thermoelectric properties of manganese-doped p-type skutterudites CeyFe_{4-x}Mn_xSb₁₂, *Funct. Mater. Lett.* 6 (5) (2013) 1340003.
- [37] L. Pan, Y. Lang, L. Zhao, D. Berardan, E. Amzallag, C. Xu, Y. Gu, C. Chen, L.-D. Zhao, X. Shen, Y. Lyu, C. Lu, Y. Wang, Realization of n-type and enhanced thermoelectric performance of p-type BiCuSeO by controlled iron incorporation, *J. Mater. Chem. A* 6 (27) (2018) 13340–13349.
- [38] J. de Boor, U. Saparamadu, J. Mao, K. Dahal, E. Mueller, Z. Ren, Thermoelectric performance of Li doped, p-type Mg₂(Ge,Sn) and comparison with Mg₂(Si,Sn), *Acta Mater.* 120 (2016) 273–280.
- [39] Y. Zhang, Z. Li, S. Singh, A. Nozariasbmarz, W. Li, A. Genc, Y. Xia, L. Zheng, S. H. Lee, S.K. Karan, G.K. Goyal, N. Liu, S.M.F. Mohan, Z. Mao, A. Cabot, C. Wolverton, B. Poudel, S. Priya, Defect-engineering-stabilized Ag₃Bi₂Te₂ with high thermoelectric performance, *Adv. Mater.* 35 (11) (2023) 2208994.
- [40] D. Kraemer, J. Sui, K. McEnaney, H. Zhao, Q. Jie, Z.F. Ren, G. Chen, High thermoelectric conversion efficiency of MgAgSb-based material with hot-pressed contacts, *Energy Environ. Sci.* 8 (4) (2015) 1299–1308.
- [41] B.Y. Pei, B. Bjorkman, B. Sundman, B. Jansson, A thermodynamic assessment of the iron - antimony system, *Calphad Comput. Coupling Phase Diagrams Thermochem.* 19 (1) (1995) 1–15.
- [42] P. Broz, F. Zelenka, J. Vrestal, A. Zemanova, A. Kroupa, J. Bursik, M. Svoboda, L. Simonikova, T. Pokorny, Experimental study and thermodynamic re-assessment of the Co-Sb system, *Calphad Comput. Coupling Phase Diagrams Thermochem.* 68 (2020) 101694.
- [43] H. Okamoto, Ni-Sb (Nickel-Antimony), *J. Phase Equilibria Diffus.* 30 (3) (2009) 301–302.
- [44] R. Todorov, T. Hristova-Vasileva, V. Katrova, V. Strijkova, A. Atanasova, G. Milushev, Formation, structure, and optical performance of AgCd/Ag₃Cd₂ phases in thin film form, *J. Mater. Sci. Mater. Electron.* 34 (13) (2023) 1093.
- [45] E.A. Brandes, G.B. Brook, Smithells Metals Reference Book, Butterworth-Heinemann, Linacre House, Jordan Hill, Oxford OX2 8DP, 1998.
- [46] R. Hea, D. Kraemer, J. Mao, L. Zeng, Q. Jie, Y. Lan, C. Li, J. Shuai, H.S. Kim, Y. Liu, D. Broido, C.-W. Chu, G. Chen, Z. Ren, Achieving high power factor and output

- power density in p-type half-Heuslers $\text{Nb}_{1-x}\text{Ti}_x\text{FeSb}$, Proc. Natl. Acad. Sci. U.S.A. 113 (48) (2016) 13576–13581.
- [47] K. Zhang, S. Liu, X. Wang, S. Wu, Q. Xiong, X. Wang, J. Chen, G. Wang, B. Zhang, H. Fu, G. Han, G. Wang, X. Lu, Y. Zhou, X. Zhou, Dual alloying enables high thermoelectric performance in AgSbTe_2 by manipulating carrier transport behavior, Adv. Funct. Mater. 34 (34) (2024) 2400679.
- [48] B. Ma, H. Ren, F. Zhang, Z. Peng, H. He, M. Cui, Z. Ge, B. Li, W. Wu, P. Liang, Y. Xiao, X. Chao, Z. Yang, D. Wu, All cubic-phase δ -TAGS thermoelectrics over the entire mid-temperature range, Small 19 (17) (2023) 2206439.
- [49] P. Sauerschnig, P. Jood, M. Ohta, Improved high-temperature material stability and mechanical properties while maintaining a high figure of merit in nanostructured p-type PbTe-based thermoelectric elements, Adv. Mater. Technol. 8 (5) (2023) 2201295.
- [50] Y.-C. Shi, J. Yang, Y. Wang, Z.-G. Li, T.-Y. Zhong, Z.-H. Ge, J. Feng, J. He, Highly effective solid solution towards high thermoelectric and mechanical performance in Bi-Sb-Te alloys via Trojan doping, Energy Environ. Sci. 17 (6) (2024) 2326–2335.

Effective diffusion barrier layer enables a robust CdSb-based thermoelectric single-leg device

Shanshan Hu[#], Min Liu[#], Long Yang, Zhiwei Chen, Jun Luo, Wen Li*, Yanzhong Pei*

Interdisciplinary Materials Research Center, School of Materials Science and Engineering, Tongji University, 4800 Caoan Road, Shanghai, 201804, China.

[#]These authors contributed equally.

*Email: liwen@tongji.edu.cn (WL), yanzhong@tongji.edu.cn (YP)

Efficiency measurements

The output power can be calculated using the formula $P=IV$, where I represents the current and V stands for the output voltage. The maximum output power can be obtained by varying the load resistance and measuring the corresponding values of I and V . According to the heat-flow meter, the heat flow is determined by the temperature difference, dimensions, and thermal conductivity of copper using the following equation.

$$Q = \frac{\kappa_{Cu} A_{Cu}}{L_{Cu}} \Delta T_{Cu} \quad (1)$$

where Q , A_{Cu} , L_{Cu} , $\Delta T_{Cu}=T_3-T_4$ and κ_{Cu} are the heat flow, the cross-section area of the heat-flow meter, the distance between the thermocouples, the temperature difference and the thermal conductivity of copper, respectively. The average κ_{Cu} of ~386 W/m-K is used for determining the heat flow¹.

The conversion efficiency (η) is given by the following equation:

$$\eta = \frac{P}{P+Q} \quad (2)$$

The maximum conversion efficiency (η_{max}) can be obtained by varying the load resistance and measuring the corresponding output power and heat flow. To minimize the system error, each parameter (including temperature, voltage and current) was measured 30 times for averaging.

Prediction of device properties according to the measured properties of the material:

The internal resistance (R_{in}) of the single-leg device at different temperature (T) is estimated by:

$$R_{in} = \frac{l}{A} \frac{\int_{T_c}^{T_h} \rho(T) dT}{\Delta T} \quad (3)$$

where l is the height and A is the cross-sectional area of the single leg, $\rho(T)$ is the resistivity of the single leg.

The open-circuit voltage (V_{oc}) of the single-leg device is estimated by:

$$V_{oc} = \int_{T_c}^{T_h} S(T) dT \quad (4)$$

where $S(T)$ is the Seebeck coefficient of the single leg.

The theoretical conversion efficiency (η) of the single-leg device is estimated by:

$$\eta = \frac{T_h - T_c}{T_h} \frac{\sqrt{1 + Z\bar{T}} - 1}{\sqrt{1 + Z\bar{T}} + \frac{T_c}{T_h}} \quad (5)$$

where $Z\bar{T} = \frac{\int_{T_c}^{T_h} Z(T) T dT}{T_h - T_c}$, ZT is the figure of merit of the leg.

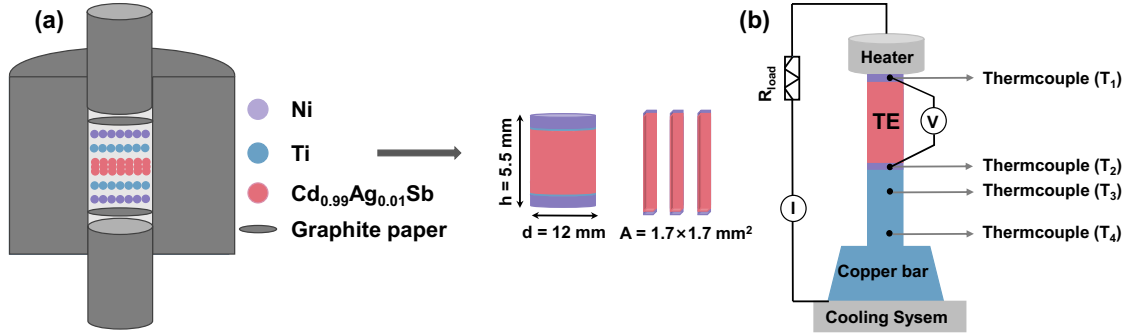


Fig. S1. Schematics of single-leg fabrication (a) and conversion efficiency measurement for Cd_{0.99}Ag_{0.01}Sb/Ti/Ni device.

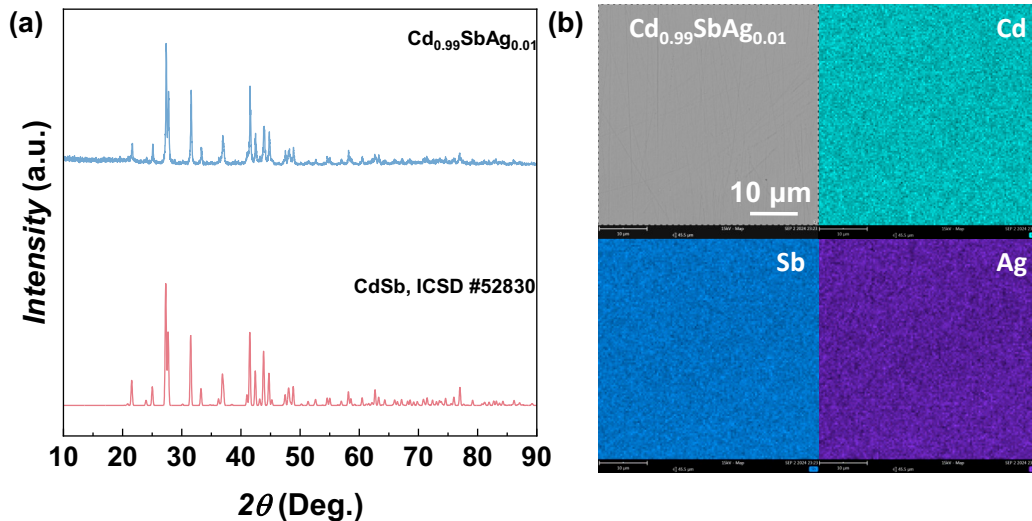


Fig. S2. Room temperature powder X-ray diffraction (XRD) pattern (a) and scanning electron microscope (SEM) image with corresponding energy dispersive spectrometer (EDS) mappings for Cd_{0.99}Ag_{0.01}Sb.

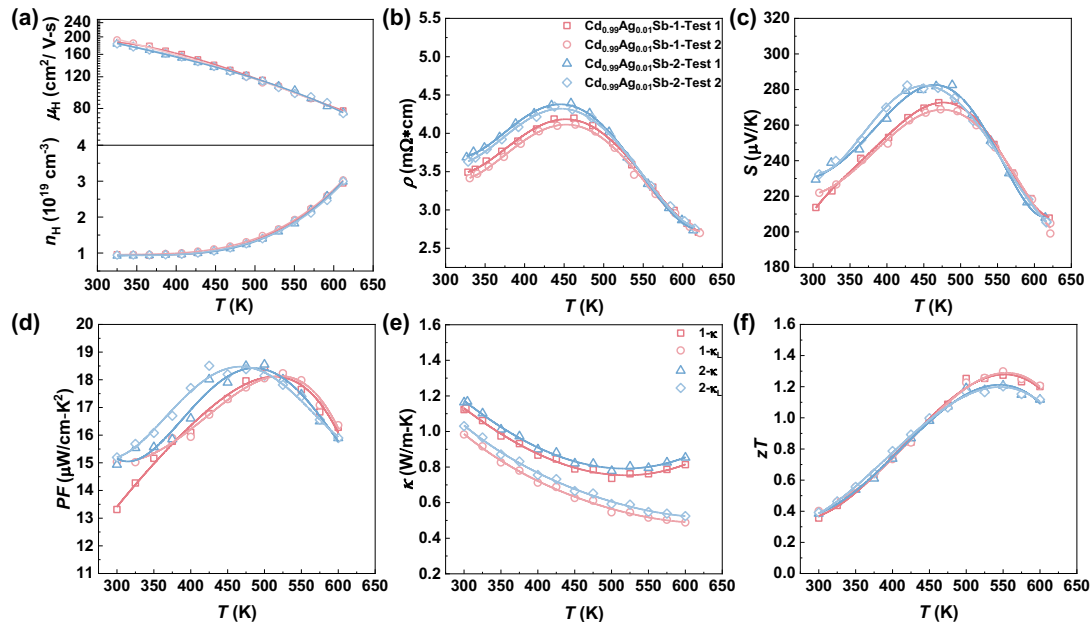


Fig. S3. Temperature dependent Hall carrier concentration (n_H) and Hall mobility (μ_H) (a), resistivity (ρ , b), Seebeck coefficient (S , c), power factor (PF , d), total (κ) and lattice (κ_L) thermal conductivity (e) and figure of merit (zT , f) for Cd_{0.99}Ag_{0.01}Sb.

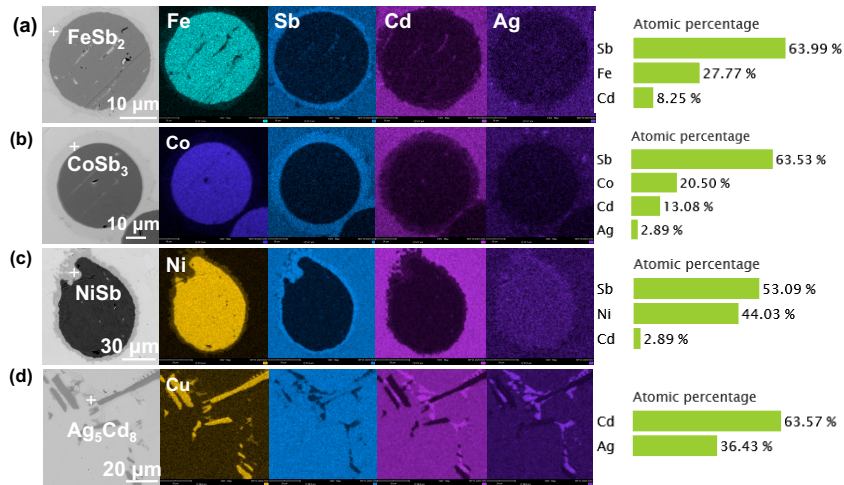


Fig. S4. SEM images and EDS analyses of the interfaces between $\text{Cd}_{0.99}\text{Ag}_{0.01}\text{Sb}$ and four kinds of metals (Fe, Co, Ni and Cu) without aging.

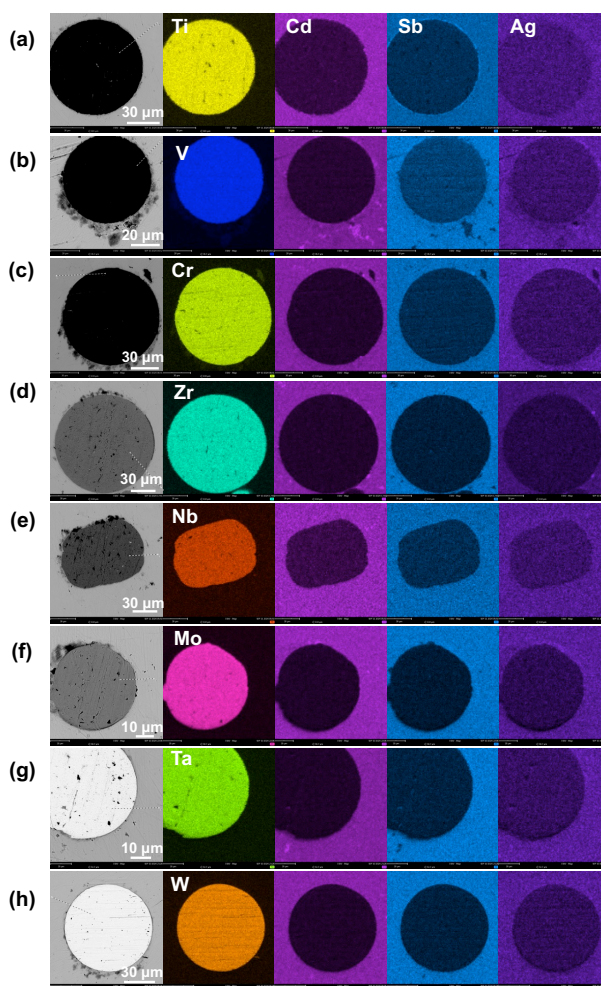


Fig. S5. SEM images and corresponding EDS mappings of the interfaces between $\text{Cd}_{0.99}\text{Ag}_{0.01}\text{Sb}$ and eight kinds of metals (Ti, V, Cr, Zr, Nb, Mo, Ta and W) with aging at 573 K for 400 h.

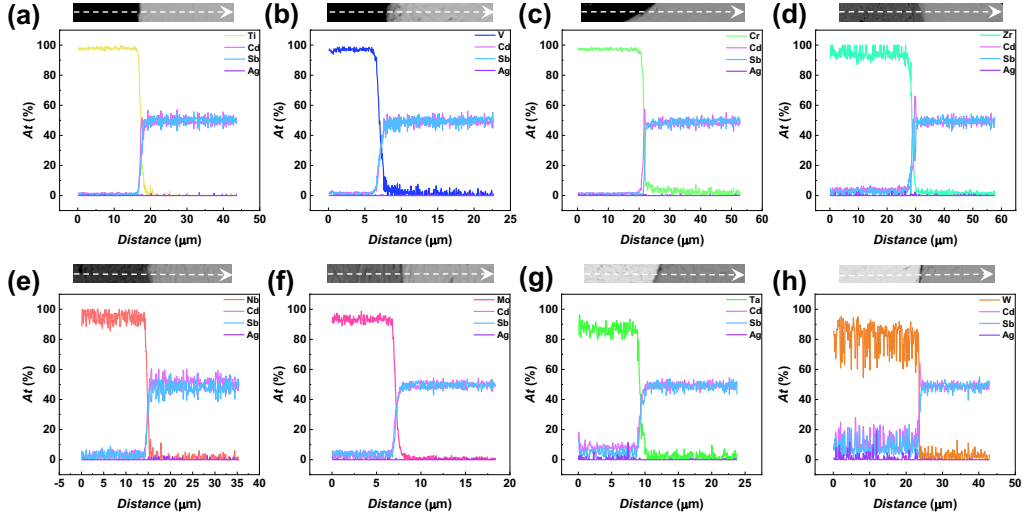


Fig. S6. EDS compositional line scans of the interfaces between $\text{Cd}_{0.99}\text{Ag}_{0.01}\text{Sb}$ and eight kinds of metals (Ti, V, Cr, Zr, Nb, Mo, Ta and W) with aging at 573 K for 400 h.

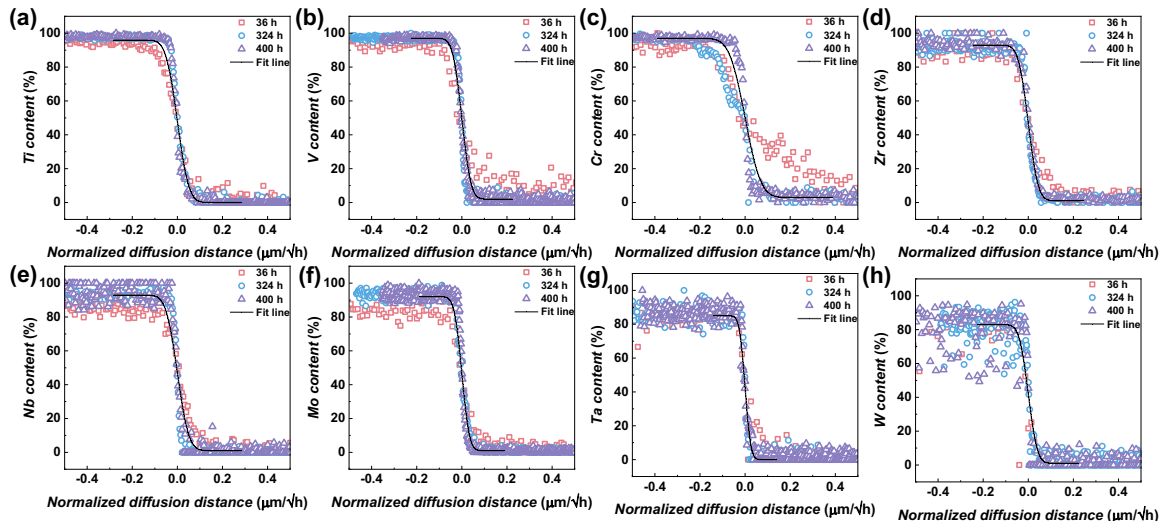


Fig. S7. Metal concentration versus normalized diffusion distance (x/\sqrt{t}) for Ti, V, Cr, Zr, Nb, Mo, Ta and W in $\text{Cd}_{0.99}\text{Ag}_{0.01}\text{Sb}$, with comparisons to the predictions (solid curves) according to the second Fick's law of diffusion.

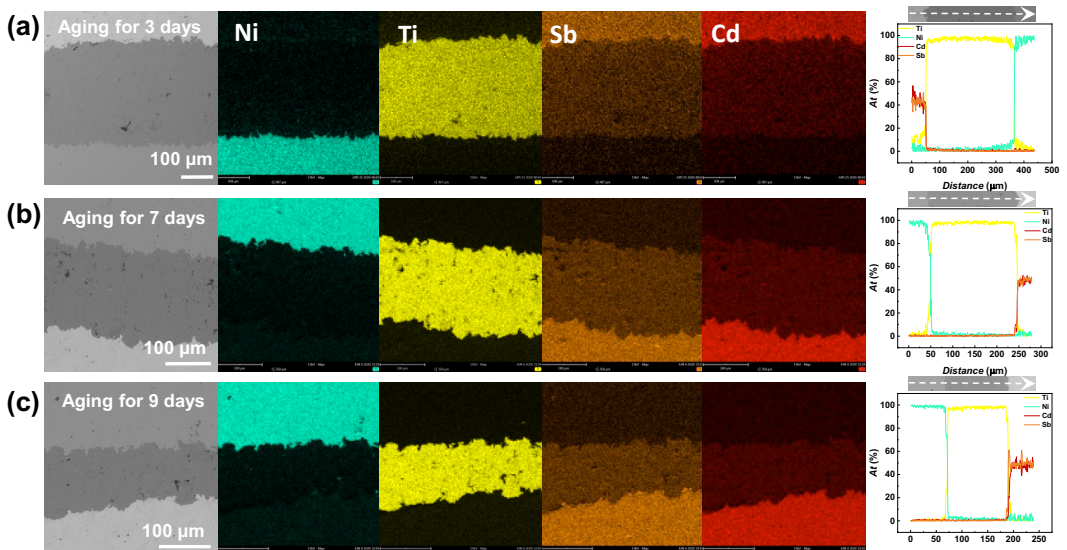


Fig. S8. SEM images with corresponding EDS mapping and line scan of Ni/Ti/Cd_{0.99}Ag_{0.01}Sb joint with aging at 573 K for 72, 168 and 216 hours.

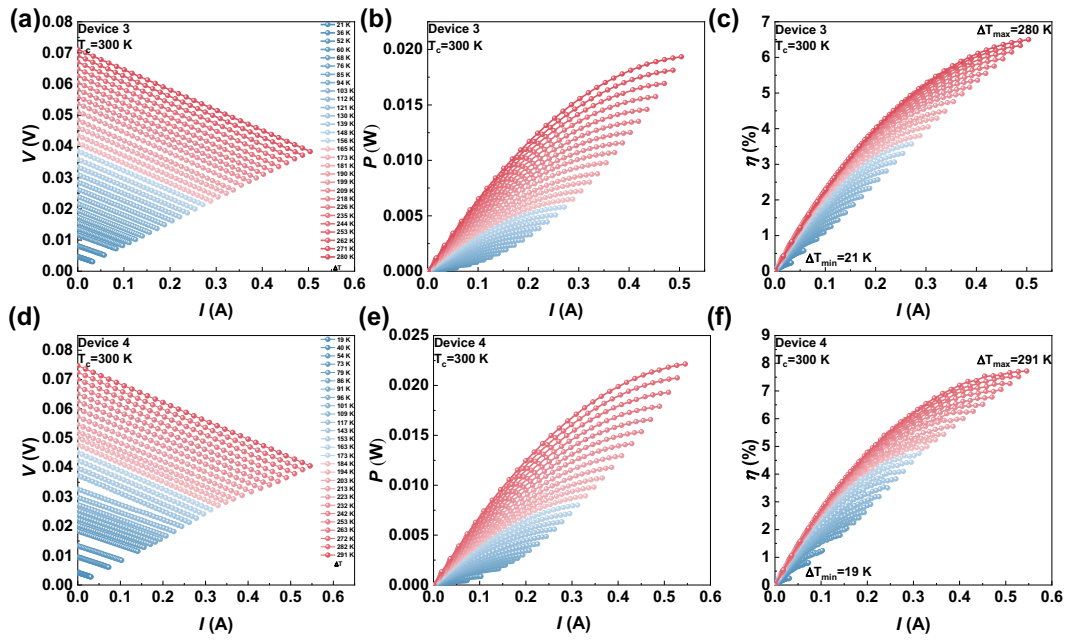


Fig. S9. Output voltage (a, d), output power (b, e) and efficiency (c, f) versus current for $\text{Cd}_{0.99}\text{Ag}_{0.01}\text{Sb}$ devices with (a, b, c) and without (d, e, f) barrier layers and electrodes.

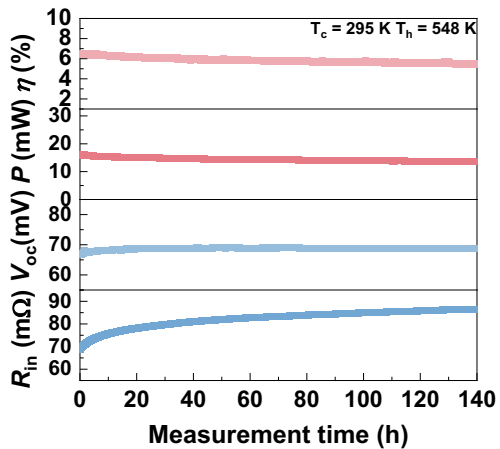


Fig. S10. Stability measurement of Ni/ $\text{Cd}_{0.99}\text{Ag}_{0.01}\text{Sb}/\text{Ni}$ single-leg device.

References

1. Liu, M.; Zhang, X.; Tang, J.; Chen, Z.; Li, W.; Pei, Y., Screening metallic diffusion barriers for weldable thermoelectric devices. *Science Bulletin* **2023**, *68* (21), 2536-2539.